DIAGNOSTICS AND INSTURMENTATION FOR FEL

M. E. Couprie, Service de Photons, Atomes et Molécules, Saclay, and Laboratoire d'Utilisation du Rayonnement Électromagnétique, Orsay, France

Abstract

Free Electron Laser are coherent sources of radiation based on the interaction of a relativistic electron beam in an undulator field. According to the energy of the accelerator, they presently cover a wide spectral range, from the infra-red to the VUV. FELs combine the diagnostics of typical laser systems (for the measurement of spectral and temporal characteristics, the transverse mode pattern, the polarisation) and the diagnostics of relativistic electron beams. The electron beam is characterised in order to evaluate and control the FEL performances, but also in order to measure the effect of the FEL on the electron beam. The FEL characteristics are monitored with various types of detectors, depending mainly on the spectral range. Diagnostics for Linac based Infra Red FELs and storage ring FELs in the UV-VUV will be described. Particular instrumentation, required for FEL operation, such as the optical resonator, possible diagnostics inside the undulator will also be analysed.

1 INTRODUCTION

The development of FELs followed the pioneering ideas [1] and experiment led by J. M. J. Madey in 1977 in the infra-red at Stanford on a linear accelerator [2]. The second FEL oscillation was then achieved in Orsay, on the storage ring ACO, in the visible range in 1983 [3]. Since then, a large number of simple and advanced undulators have been built and integrated into FELs. FEL facilities provide a fully coherent tuneable light in a wide spectral range for scientific applications in various domains.

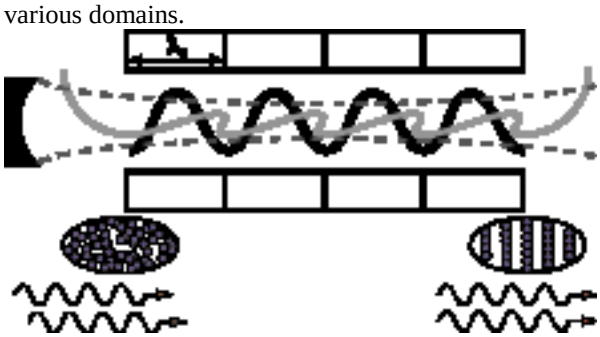

Fig.1 FEL principle

As illustrated in figure 1, Free Electron Laser (FEL) oscillation results from the interaction of an optical wave with a relativistic electron beam circulating in the periodic ppermanent magnetic field of an undulator (period λ_0 and peak magnetic field B_0 along the vertical direction y). The relativistic particles are transversely accelerated and emit synchrotron radiation, at the resonant wavelength λ_r and its harmonics :

$$\lambda_r = \frac{\lambda_0}{2\gamma^2}\left(1 + K^2/2\right) \qquad (1)$$

with the deflection parameter K = 0.94 λ_0(cm) B_0(T) and γ the normalised energy of the electrons. The interaction between the optical wave and the electron bunch occurs along the undulator progression. Generally, an optical resonator, the length of which is adapted to the recurrence of the electron bunches, allows the radiation to be stored and the interaction to take place at each passage. The optical wave and the charged particles exchange energy, which can lead to a modulation of the electronic density at the wavelength of light (microbunching), phasing the emission and reinforcing the coherence of the produced radiation. An additional second order energy exchange between the optical wave and the electron beam leads to a non linear amplification of the stored towards saturation is reached (the gain of the system becomes equal to the cavity losses); meanwhile the spectral and temporal widths narrow. Through the system constituted by the relativistic electron beam in the undulator, coherent harmonics can be produced from an external laser source or from the FEL itself.

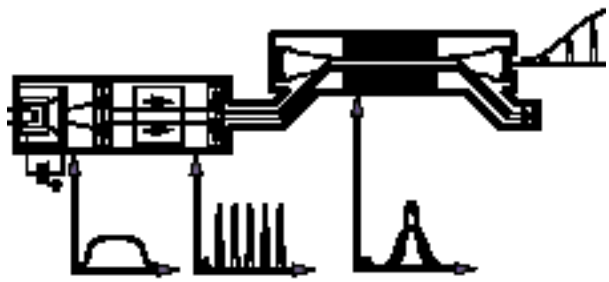

Fig. 2 : LINAC based FEL

By changing the deflection parameter K or the electron energy, one changes the resonant wavelength. As result, the FEL is intrinsically a tuneable source of radiation. The undulator period is typically a few cm long, therefore the higher the electron energy, the shorter the wavelength. FELs on low energy accelerators (MeV range) operate in the microwave and far infra red ranges, FELs on intermediate energy accelerators (50 MeV) cover the mid infra-red and ultra-violet ranges, and systems on higher energy accelerators (100 MeV-GeV) reach the UV, VUV and X-ray ranges. The gain is lower for higher energies, and optics are easily available in the infra-red. Therefore, the FEL was developed faster in the infrared (the first FEL oscillation was achieved in the UV in 1988 in

ovosibirsk [4]) and the shortest wavelength was generated by coherent harmonics at 100 nm on Super-ACO in 1990 [5]. Very recently, amplification was observed in the SASE regime on the TESLA-TTF experiment at 80 nm [6].

The most popular type of accelerator used in the infra-red is the conventional RF linear accelerator (LINAC) (see fig.2). The electron beam, produced by a cathode, consists in a series of several µs pulses, emitted at a repetition rate ranging between 1 and 100 Hz. Following the passage of the beam through the RF accelerating structure, the macropulse is bunched into a few thousands of picosecond micropulses, with a spacing given by the RF field wavelength (typically 0.3-1 ns). A superconducting RF LINAC provides longer macropulses (typically 1 ms). Recent use of a photocathode produces very short micropulses (in the femtosecond range). The electron beam goes to a beam dump, and a "new" bunch interacts at each passage with the FEL. Several user facilities are currently operating in the infra-red, exploiting the high average power associated to the wide tunability for scientific applications. Average FEL power as high as a few hundred watts in the infra-red has been recently obtained at Jefferson Lab. (USA) [7] and JAERI (Japan) [8]. In order to insure a proper synchronisation between the optical pulse which reflects back and forth between the mirrors and the succesive bunches, the distance between the mirrors should be an integer of the electron bunch distance.

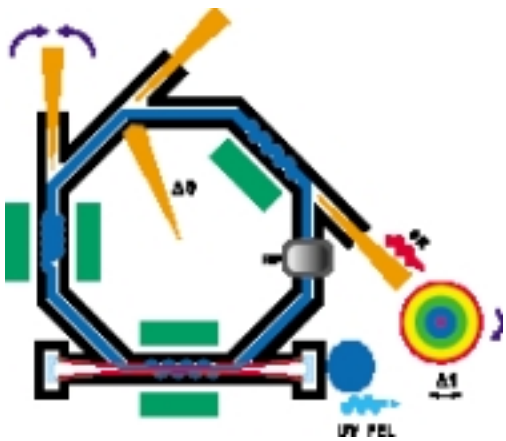

Fig. 3 : Storage ring based FEL

In the UV range, the majority of FELs are built on storage rings (see fig.3). In that case, the beam is recirculated from pass to pass and keeps memory from its interaction with the FEL. Besides, the FEL radiation can be coupled with synchrotron radiation, with which it is naturally synchronised, for pump-probe two-colour experiments [9]. In this case, the storage ring FEL (SRFEL) reproduces the pulsed MHz structure (although the filling should be limited to a few bunches in order to avoid inter-bunch longitudinal instabilities). Unlike LINACs, one may operate a large circulating current in the storage ring (few hundred mA) which implies a large circulating power (1 GW). The power of a storage ring FEL is nevertheless limited by the electron energy spread induced by the electron beam.

2 CONSTITUTING ELEMENTS OF THE FEL

2.1 Electron beam characterization

The usual electron beam characterisations both for LINACs and storage ring are used to determine the beam transverse and longitudinal dimensions, the energy spread. They are required for a careful gain evaluation. In addition, the stability of the electron bunch should be carefully checked. The usual accelerators measurements are not detailed here, but particular experimental set-up were proposed and tested with FEL accelerators. For instance, sub-picosecond electro-optic measurement of relativistic electron pulses were demonstrated on FELIX [10]. Using an ultrafast electro-optic sensor close to the electron beam, the longitudinal profile of the electric field was measured with subpicsecond time resolution and without time-reversal ambiguity. The electric field induces abirefringence in the electro-optical crystal (Zn-Se for example), which is probed by a synchronised Ti:Sapphire pulse.

2. 2.2 Undulator

The choice of the insertion device for the FEL operation provides some specific constraints. As the FEL and the electron beam should interact along the undulator, additional detectors can be installed. Besides, an optical klystron [11] is generally employed for a storage ring FEL, in order to artificially enhance the gain. The optical klystron consists of two undulators separaed by a dispersive section creating a wide wiggle of magnetic field. Its spectrum is then the result of the interference of the two undulators radiation spectra, as for the Young slits. From the depth of the modulation rate (the equivalent to the optical contrast), one can deduce the energy spread of the beam [12].

2.3 Optical cavity

Various characterisations can be performed on the mirrors of the optical resonator. The roughness, which defines the scatter losses can be measured by a picometer profilemeter developed at ESPCI (see fig. 4) and by a Zygo apparatus. Cavity losses can be measured using the Herbelin method [13], the absorption of the layers can be characterised using the photothermal deflection method [13]. Transmission can be checked with a spectrometer. Different optical techniques are

used in order to measure the mirror radius of curvature, for the resonator stability.

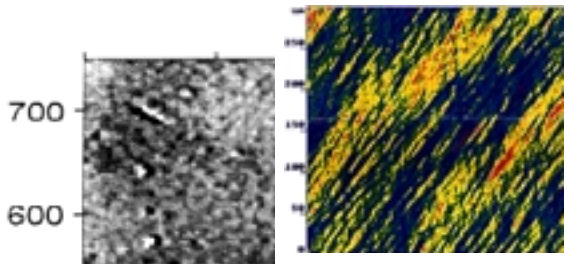

Fig. 4 : Mirror roughness measurement. On the left, 3.4 Å roughness measured with a picometer interferometer at Ecole de Physique et Chimie Industrielles (paris), on the right, 8.7 Å characterised with a ZYGO interferometer at SESO on a different sample.

3 FEL CHARACTERIZATION

3.1 Intensity measurements

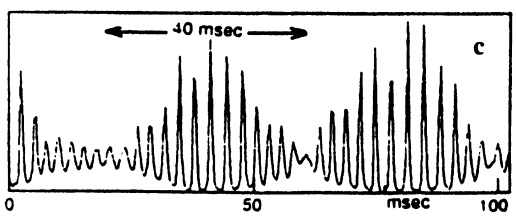

Fig. 5: Evolution of the macrotemporal structure of the Super-ACO FEL in presence of a low frequency modulation.

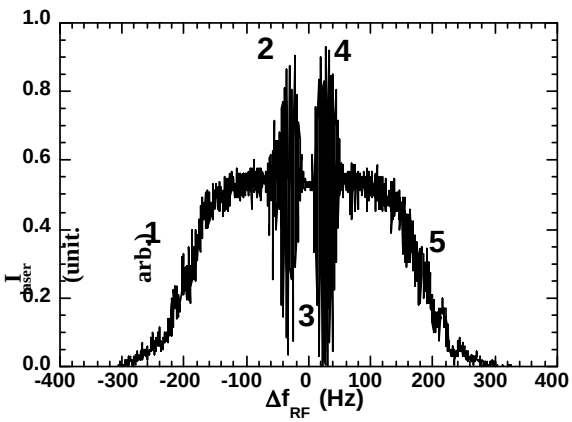

Fig.6: Super-ACO FEL intensity versus the difference between the revolution frequency of the electrons in the ring and the round trip time of the photons in the optical resonator. I = 90 mA.

The intensity measurements depend on the spectral range. In the Infra-red, Hg-Cd-Te detectors are used. In the visible down to the VUV, photomultipliers (PM) can be employed (see fig. 5). Such detectors allow to follow the behaviour of the FEL when one parameter is changed. In fig.6, a ramp is changing the tuning condition of the FEL (the synchronisation between the optical pulses bouncing in the resonator and the electron bunches stored in the ring). The signal of the PM versus the frequency changed is acquired on an ocilloscope. One can then distinguish five zones, zone three for a CW laser around perfect tuning, zones two and four where the laser is pulsed, and zone 1 and 5 where the laser is again CW.

3.2 Spectral characterisation

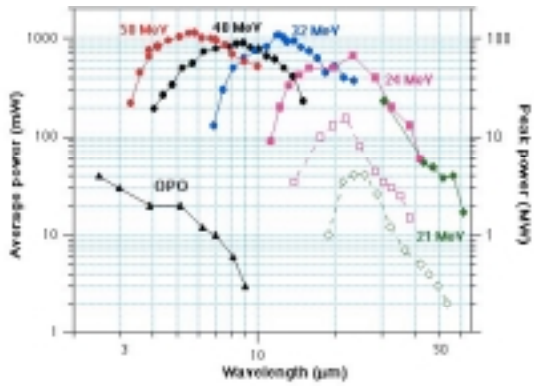

Fig. 7 : Intensity measurement of the CLIO infra-red FEL

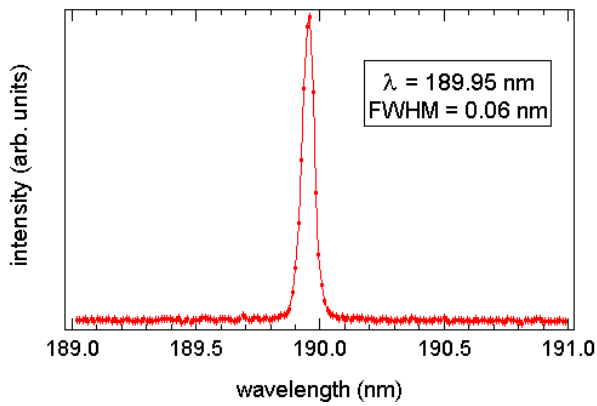

Fig. 8 : Spectral line of the ELETTRA FEL at 190 nm (the world record of the shortest wavelength in the FEL oscillator mode, 2001)

Grating monochromators are generally used for characterising the spectral features of the FELs. The light, after a slit selection, is sent to a system of gratings, which separates its spectral content. The exit light detector depends on the spectral range of the FEL source. The chosen photocathode is selected according to the spectral range. An example of CLIO tuneability in the infra-red is shown in fig. 7. From these measurements, it appears than the relative spectral range typically is in the 0.1-1% range for an Infra-red LINAC based FEL, and of 0.01 % for a storage ring FEL. A measurement of the spectral width of the ELETTRA FEL in the VUV at 190 nm is given

in fig. 8. Further resolution can be achieved by using a scanning Fabry-Perot interferometer [14].

3.3 Temporal measurements

Different temporal detector are used according to the temporal width of the phenomenon to be studied. Nanosecond down to several dizains of picosecond can be measured with photomultipliers and fast photodiodes. The sensitive material of the photocathode is selected according to the spectral range. Picosecond range phenomena are characterised by stroboscopic techniques such as the dissector for phenomenon having a fixed period of reproducibility, or with a streak camera. In that case, the light pulse strikes a photocathode which yields an electronic pulse proportional to the incident intensity. In a streak camera, this pulse is then swept very quickly by two electrodes which are triggered at the frequency of the accelerator (synchroscan tube). It provides different fast sweep time scales in the ps up to the ns range. The typical resolution is of 2ps, but up to 500 fs can be reached in the single sweep mode. In addition, for double sweep streak cameras, a horizontal slow sweep shifts light pulses on the CCD (Charge Couple Device) screen versus different sweep ranges available between 100 ns and 1 s. The light intensity profile is provided by a vertical cut of the image (see fig. 9). The evolution of the longitudinal distribution in time is followed along by the horizontal time axis.

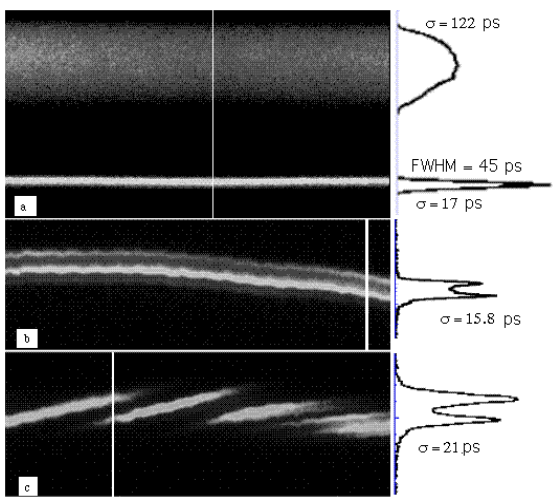

fig. 9 : Example of the Super-ACO FEL (Orsay). Cw FEL (area 3), 1a, Vertical scale = 1.7 ns, Horizontal scale = 1 ms; 1b, 300 ps, 10 ms; 1c, 300 ps, 10 ms; the current, I = 50 mA. The laser temporal distribution with their width RMS, associated to vertical slices for each image, are also plotted.

The different detuning zones of operation of the FEL can then be followed using the double sweep streak camera, as shown in Fig. 10.

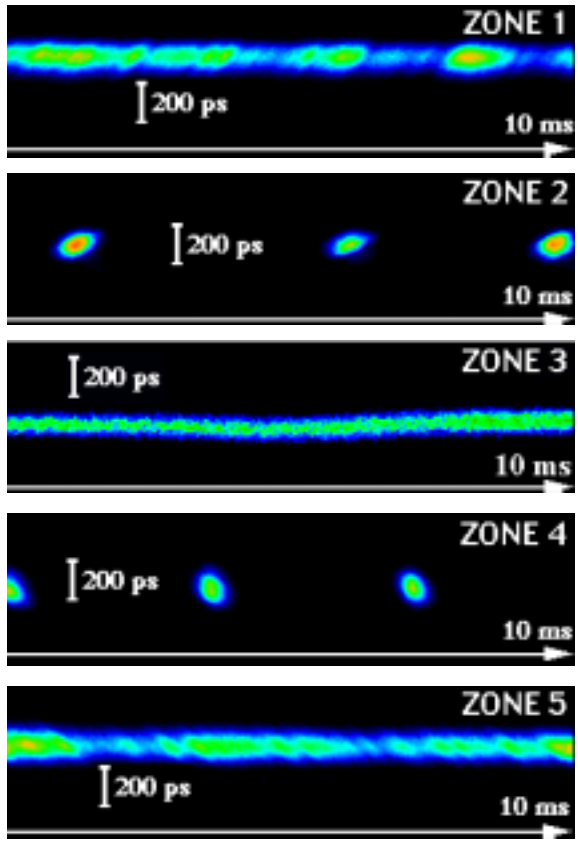

Fig. 10 : Super-ACO FEL pulse measured for different detuning with the double sweep streak camera (Hamamatsu). zone 1 : Δf_{RF} = -50 Hz, zone 2 : Δf_{RF} = -10 Hz, zone 3 : Δf_{RF} = 0 Hz, zone 4 : Δf_{RF} = +10 Hz, zone 5 : Δf_{RF} = +50 Hz

In a dissector [15], the electron beam from the photocathode is deflected onto the plane of a slit by a radio frequency voltage. For a period of deflection voltage equal or multiple of the repetition rate of the pulse, only a portion of the electron distribution goes through the slit, whose width determines principally the geometrical resolution of the device. Subsequently this part of electrons is amplified by a series of dynodes and transformed in an electric signal that is sent to a scope. A low frequency sweeping voltage superposed to the radiofrequency deflection one completes the measurement by scanning the whole electron density distribution. As a result, the characteristic time intervals observed on the scope are correlated to the real time intervals by a known fixed calibration factor. Besides, the frequency of the sweeping voltage gives the measurement time rate, which can be as high as 5 kHz. The dissector signal can then processed electronically, and the position of the FEL pulse can be measured with respect to a reference position as shown in fig. 11a, versus the detuning. Fig. 11b gives the imultaneously measured detuning curve, using the same trigger from the ramp generator.

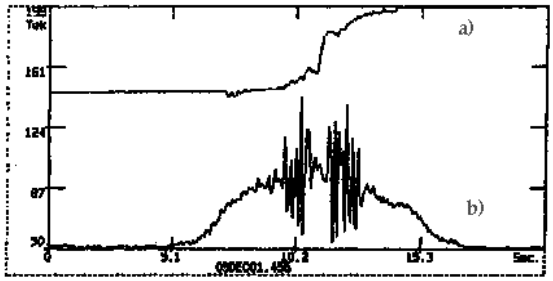

Fig.11: Super-ACO FEL position and intensity versus the difference between the revolution frequency of the electrons in the ring and the round trip time of the photons in the optical resonator. I = 90 mA.

A detuning curve can also be plotted with the double sweep streak camera by applying a proper trigger to the dual sweep tube, as shown in fig. 12.

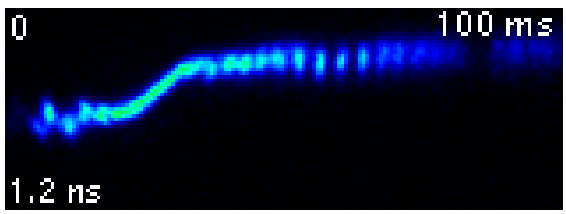

Fig. 12 : Detuning curve of the Super-ACO FEL measured with the double sweep streak camera.

Femtsosecond range measurements can be achieved with autocoreelators [16]. Rapid-scanning cross-correlation techniques probing the field birefringence in ZnTe with a 10 fs Ti:Sapphire laser have also been demonstrated [17]. Frequency resolved optical gating (FROG) measurements on the Superconducting Accelerator (SCA) mid-IR free-electron laser (FEL) have also been at Stanford [18]. FROG retrieves complete amplitude and phase content of an optical pulse.

3.4 Transverse modes measurements

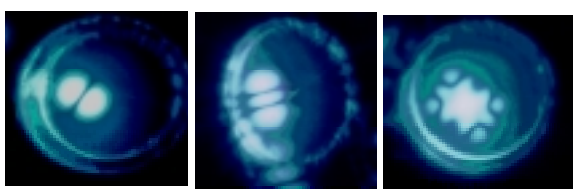

Fig. 13 : Transverse modes observed on the Super-ACO FEL, resulting from a cavity misalignement with respect to the magnetic axis of the undulator (TEM01, TEM02, TEM23).

The transverse mode pattern can be measured with a CCD camera. The profile can then be analysed. Example of different modes of the Super-ACO FEL are shown in fig. 13.

3.5 Polarisation measurements

The FEL polarization depending on the undulator type (planar, helical), it is measured with standard analysers and polarisers.

4 FEL INDUCED MODIFICATION OF THE ELECTRON BEAM

The FEL and the electron beam can be measured together. The beam stabilisation induced by the FEL in presence of saw-tooth instability is shown in fig. 14.

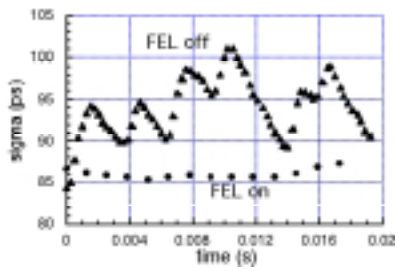

Fig. 14 : Super-ACO FEL stabilizing the electron measured with a double sweep streak camera.

5 CONCLUSION

FEL combine the diagnostics of accelerator and of conventional lasers. They could themselves even be considered as machine diagnostics since they are extremely sensitive to the stability of the accelerator.

REFERENCES

[1] J.M.J. Madey *Jou. Appl. Phys*., **42**, 1906 (1971).;
[2] J.M.J. Madey *Phys. Rev. Lett.*, **36**, 717 (1976).
D.A.G. Deacon et al, *Phys. Rev. Lett.*, **38**, 892-894,1977
[3] M. Billardon et al, *Phys. Rev. Lett*. **51**, 1652 (1983)
[4] Kulipanov G.N et al *Nucl. Instr. Meth*., A**296**, 1-3 (1990)
[5] R. Prazeres et al *Europhys. Lett*., **4** (7), 817-822 (1987);
[6] J. Rossbach Proced. EPAC, Austria, 26-30 June 2000
[7] S. Benson et al. Nucl. Inst. Meth. A 429 (1999) 27-32
[8] E.J. Minehara et al Nucl. Inst. Meth. A 429 (1999) 9-11
[9] M. Marsi et al, *Appl. Phys. Lett.* **70**(7) (1997) 895-897;
[10] X. Yan et al Phys. Rev. Lett.85(16), 2000, 3404-3407
[11] N.A.Vinokurov, A.N. Skrinsky Preprint INP77.59 Novossibirsk 1977; P. Elleaume: Optical Klystron, J. Phys. (Paris) 44, C1-353 (1983)
[12] R.J. Bakker et al *Proc. EPAC'96, S. Myers*, A. Pacheco, R.R. Pascual, Ch. Petit-Jean Genaz, J. Poole Ed. (Inst. of Phys. Publishing, Bristol and Philadelphia, (1996) 667-669
[13] D. Nutarelli et al. 20th Intern. FEL Conf 1998, G. R. Neil and S.V. Benson (Eds.) 1999 Elsevier Science B.V. II-63
[14 T. Hara et al *Nucl. Inst. Meth.* **A375** (1996) 39-45
[15] E.I. Zinine *Nucl. Instr. Meth.*, **A208**, 439-441, 1983.
[16] F. Glotin et al, Phys. Rev. Lett., **71**, 2587 (1993)
[17] G. M. H. Knippels et al Phys. Rev. Lett. 83 (8), Aug. 1999 1578-1581